ACCEPTED MANUSCRIPT

Physics of Fluids

This is the author's peer reviewed, accepted manuscript. However, the online version of record will be different from this version once it has been copyedited and typeset.

PLEASE CITE THIS ARTICLE AS DOI: 10.1063/5.0058693

Novel modeling approach for fiber breakage during molding of long fiber-reinforced thermoplastics

Abrahan Bechara[1], Sebastian Goris[1], Angel Yanev[2], Dave Brands[2], Tim Osswald[1]

[1]Department of Mechanical Engineering, University of Wisconsin Madison, Madison, WI

[2]Global Application Technology, SABIC, AH Geleen 6160, The Netherlands.

Abstract

Long fiber-reinforced thermoplastics (LFTs) are an attractive design option for many engineering applications due to their excellent mechanical properties and processability. When processing these materials, the length of the fibers inevitably decreases, which ultimately affects the mechanical performance of the finished part. Since none of the existing modeling techniques can accurately predict fiber damage of LFTs during injection molding, a new phenomenological approach for modeling fiber attrition is presented. First, multiple controlled studies employing a Couette rheometer are performed to determine correlations between processing conditions, material properties, and fiber length reduction. Results show shear stress and fiber concentration impact fiber damage. Based on these findings, a phenomenological model to predict breaking rate and unbreakable length of a fiber under giving conditions is developed. The model is based on beam theory with distributed hydrodynamic stresses acting on a fiber. Fiber-fiber interactions are accounted for and correlated with the fiber volume fraction via a fitting parameter. The model tracks both the number-average and weight-average fiber length during processing, which can in turn be used to extract the fiber length distribution.

1 Introduction

The use of injection-molded long-fiber thermoplastic composites (or LFTs) has been rapidly increasing in the past decade, mainly due to the market push for more fuel-efficient vehicles as well as electric vehicles. While the transportation industry constitutes 80% of LFTs' world usage, their use is also increasing in applications such as durable consumer appliances, electronics, and sporting goods [1,2]. Since their advantage is the high aspect ratio of the fibers, a primary concern for manufacturers is preserving the fibers' length throughout the molding process [3]. Initial fiber length in LFT pellets typically ranges from 10 to 15 mm. Fiber length measurements suggested a remaining average fiber length in the molded part in the 1 to 3 mm range [4–8].

The impact of processing variables on fiber attrition at different stages of the molding process has been the focus of numerous studies. Bailey and Kraft found that most damage occurs during plastication, as did Lafranche et al. and others [4–7]. Most notably, they found higher fiber lengths in the core region than the skin region in molded parts, also observed in other studies, which suggests that the characteristic flow regime during mold filling causes uneven fiber breakage [5,9]. These findings go hand in hand with recent findings on the inhomogeneous fiber density distribution in injection molding of LFT [10].

Rohde et al. performed a full factorial DOE varying processing parameters such as injection speed, screw back pressure, holding pressure, and screw speed, where their results clearly show a significant impact of back pressure on fiber length [7]. Most processing variables had no significant statistical impact on fiber length, while an increase in backpressure from 50 to 80 bar reduced the fiber length in the mold cavity by

15 July 2024 18:12:51

ACCEPTED MANUSCRIPT
Physics of Fluids
This is the author's peer reviewed, accepted manuscript. However, the online version of record will be different from this version once it has been copyedited and typeset.
PLEASE CITE THIS ARTICLE AS DOI: 10.1063/5.0058693
AIP Publishing
15 July 2024 18:12:51

approximately 30%. Nevertheless, the authors state that it is difficult to isolate the mechanisms that cause fiber attrition due to the complex phase change and shear history present in the injection molding process.

Inoue et al. found that the screw design in the compression zone has a substantial impact on fiber breakage [11]. They observed that an optimized screw design (Dulmadge [12] with a variable pitch) could reduce the fiber breakage compared to a standard screw. Von Turkovich et al. conducted compounding experiments with short-fiber thermoplastic composites (or SFTs) and found that most of the fiber damage occurred in the compression zone [13]. Based on their results, they concluded fiber concentration and initial fiber dispersion had no visible impact on the fiber length.

More fundamental studies on fiber motion were conducted by Forgacs and Mason, employing a Couette device and subjecting single fibers to simple shear flow [14,15]. They used Burger's formulation along with Euler's beam theory, to derive an equation to estimate the critical product $\dot{\gamma}\eta$, at which a fiber would buckle under compressive stresses [16]. By increasing either the aspect ratio of the fibers or the product $\dot{\gamma}\eta$, Forgacs and Mason identified various orbits of rotation; Figure **1** summarizes their findings.

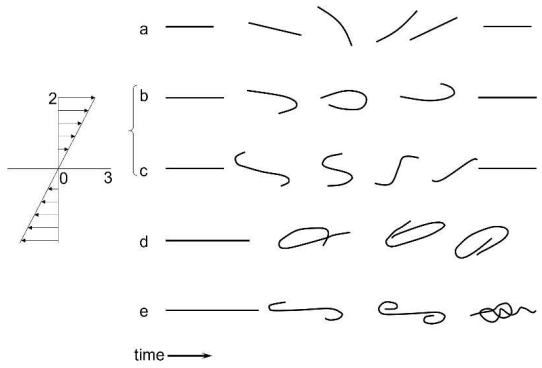

Figure 1. Types of fiber motion in simple shear flow as flexibility increases from a to e. a) springy rotation, b) c) snake orbit, d) e) coiled rotation (adapted from [17]).

Using a similar device, Salinas and Pittman performed experiments with reinforcing fibrous materials, including glass fibers with aspect ratios ranging from 280 to 680 [17]. They found that fibers fractured in the snake orbit regime when the minimum radii of curvature were reached, and that only very stiff or brittle materials (carbon fiber, asbestos) were predicted to break in the springy regime. They derived an empirical expression for the critical product $\dot{\gamma}\eta$ that would cause sufficient deformation to cause rupture. These early studies on fiber motion and failure are the basis for most modeling approaches to the fiber attrition phenomena.

Shon et al. evaluated various combinations of mixing elements and their impact on fiber length reduction as a function of axial distance in a counter-rotating twin screw extruder [18]. They introduced a kinetic model in which an average fiber length, L, decreases exponentially toward a residual, or unbreakable length, L_∞, following:

ACCEPTED MANUSCRIPT
Physics of Fluids
This is the author's peer reviewed, accepted manuscript. However, the online version of record will be different from this version once it has been copyedited and typeset.
PLEASE CITE THIS ARTICLE AS DOI: 10.1063/5.0058693
AIP Publishing

$$\frac{dL}{dt} = k_f(L - L_\infty) \quad (1)$$

where, k_f is a breaking rate coefficient. They did not attempt to derive expressions for the parameters (L_∞, k_f) in their model but approached the problem by simply fitting the curve to the experimental data. Bumm et al. later extended Shon et al.'s work and derived expressions for both parameters based on Euler's buckling theory [19].

Durin et al., and Phelps et al., proposed similar models for fiber attrition during compounding and injection molding, respectively [20,21]. Rather than tracking the average fiber length changes over time, they wrote an equation of conservation for the complete fiber length distribution (FLD) based on a breakage probability. Following Forgacs and Masons' analysis, fiber buckling is determined to be the mechanism by which fibers break. A dimensionless buckling number, Bi, defines the critical conditions under which a fiber would have the highest possibility of buckling and eventually failing. This number is a function of the product $\dot{\gamma}\eta$, the fiber's stiffness and aspect ratio, given by

$$Bi = \frac{4\zeta\eta_m l_i^4}{\pi^3 E_f d_f^4} \quad (2)$$

Where, η_m is the matrix viscosity, E_f is the fiber's Young's modulus, l_i and d_f are the fiber's length and diameter. The variable ζ is the fiber's dimensionless drag coefficient and is used as a fitting parameter. These models introduce a Normal or Weibull probability distribution that determines the location along the fiber's axis where failure is likely to occur.

Kang et al., proposed a model similar to Durin's [22]. In their approach, fiber buckling leads to damage which is based on pure bending theory of simply supported beams. They compared the prediction capability to fiber breakage experiments performed with glass fiber-reinforced polypropylene (PPGF) in a parallel plate rheometer. The experiments were purposely conducted with low fiber concentration (10%wt) to minimize the effect of fiber-fiber interactions on fiber damage. Malatyali et al., also employed a similar approach to predict breakage of carbon fibers along a twin screw extruder [23]. For model verification 35%wt carbon fiber-reinforced polypropylene was used. The common denominator between these models is that fiber buckling is presumed to be the cause or initiator of failure. Also, none of these models consider fiber-fiber interactions to have influence on the fiber breakage phenomena. Phelps et al.'s model is currently the standard method for predicting fiber damage during injection molding in commercial software. And Durin et al.'s model has also been implemented in commercial software for twin-screw extrusion.

Chen et al. studied breakage on a capillary rheometer and proposed a breakage model based on the fibers' semi-flexible orientation [24]. Following Salinas and Pittman's conclusions, they argue fibers break due to large deformations when the minimum radius of curvature is reached. Their model indirectly accounts for fiber-fiber interactions by using the isotropic rotary diffusion parameter C_i in the orientation model [25].

15 July 2024 18:12:51

ACCEPTED MANUSCRIPT
Physics of Fluids
This is the author's peer reviewed, accepted manuscript. However, the online version of record will be different from this version once it has been copyedited and typeset.
PLEASE CITE THIS ARTICLE AS DOI: 10.1063/5.0058693
AIP Publishing
15 July 2024 18:12:51

Moritzer et al. conducted fiber breakage experiments under simple shear employing a Couette device and pre-compounded polypropylene with short fibers [26]. Their results corroborate Shon et al.'s proposed kinetics and showed that fiber concentration influenced both the breakage rate and the residual length L_∞. After performing a dimensional analysis, they proposed a phenomenological model which accounts for hydrodynamic stresses, fiber concentration, and fiber properties.

In recent years, direct particle simulation approaches have been used to study in detail the fiber breakage mechanisms. Sasayama et al. simulated fiber breakage under simple shear flow considering fiber-fiber interaction [27]. Their results show that the fiber length decreases with the product $\dot{\gamma}\eta$. They present an interesting depiction of how fiber-fiber interactions can lead to breakage. Chang et al. built a failure criterion based on a critical radius distribution obtained via loop test measurements, similar to Salinas and Pittman [28]. The introduction of this failure distribution in their direct particle simulation improved their fiber length prediction compared to Couette experiments. These approaches are somewhat limited due to their computational cost, so it is unlikely they will be used to predict fiber length in real components. However, they have great potential as numerical rheometers since the coupled effects of fiber orientation, fiber length and fiber concentration can be studied.

The main objective of this study is to develop a new model to predict fiber length during injection molding of long fiber-reinforced thermoplastics. First, a set of fiber damage experiments were conducted under highly controlled conditions employing a Couette rheometer. Important process and material variables are studied, and their impact on fiber damage is measured. Based on the experimental observations, this work derives a constitutive equation for fiber breakage kinetics and expressions for the model parameters based on hydrodynamic stress and mechanical failure are deduced.

2 Material and methods

2.1 Material

The material used in this work is a commercially available long glass fiber-reinforced polypropylene. The material is supplied as coated fiber pellets with a length of 15 mm, nominal glass fiber content of 20%, 30%, and 40% by weight (PPGF20, PPGF30, and PPGF40). Due to their fiber length, these materials are widely used for automotive panels and multi-wall structured panels in the construction industry. Table I lists pertinent material properties.

Table I. Typical long fiber PPGF material properties.

Material property	Value
Nominal fiber length	Pellet length
Fiber diameter [µm]	14 – 24 [29]
Density of fibers [g/cm^3]	2.56 [30]
Density of polypropylene (PP) [g/cm^3]	0.9 [30]
Modulus of fibers [GPa]	74-80 [31]
Ultimate strength of fibers [MPa]	2000-2500 [31]

2.2 Experimental

Investigating the underlying physics of fiber breakage experimentally in an injection molding process or during compounding in a twin-screw extruder is challenging because of the complex and changing flow conditions that the fibers are exposed to in the various stages of the process. In this work, a Couette rheometer was used to study fiber breakage under simple shear and controlled processing conditions [32]. The Couette rheometer dimensions were selected to be characteristic of the conditions during

ACCEPTED MANUSCRIPT
Physics of Fluids
This is the author's peer reviewed, accepted manuscript. However, the online version of record will be different from this version once it has been copyedited and typeset.
PLEASE CITE THIS ARTICLE AS DOI: 10.1063/5.0058693
AIP Publishing

plastication in injection molding, with the inner cylinder diameter being 35 mm, the annular gap being 5 mm, and the length of the annular volume being 80 mm (Figure 2). The temperature is controlled through insulated heater bands surrounding the outer cylinder and a thermocouple measuring the melt temperature. The inner cylinder is driven by a Plasti Corder™ torque rheometer (C.W. Brabender Instruments Inc., Hackensack, NJ), controlling the rotational speed.

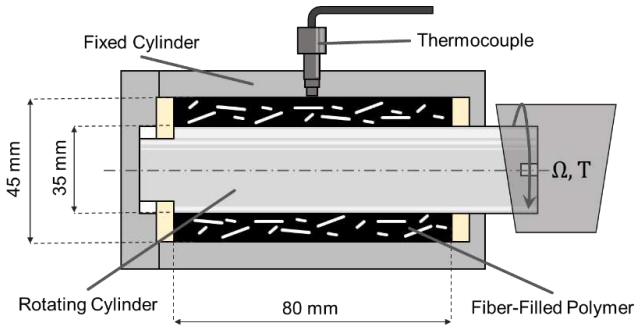

Figure 2. Illustration of the Couette rheometer setup for the study of fiber breakage.

Based on the fiber break- up model suggested by Shon et al. [18], a set of studies were conducted with the Couette rheometer to understand the kinetics of fiber length degradation and to isolate the effects that processing conditions have on the steady-state fiber length (L_∞) and the breakage rate coefficient (k_f). After each experiment, the material was removed from the Couette, and the fiber length was measured employing a technique developed at the Polymer Engineering Center at the University of Wisconsin-Madison, which is based on the method developed by Kunc et al. to determine the fiber length distribution in LFT materials [33,34].

2.2.1 Length decay over time

The first study explored the fiber length degradation over time for different processing speeds while the fiber content and melt temperature were kept constant (Table II). The material was sheared for increasing intervals of time, starting with 20s until 300s. This set of experiments allow the characterization of fiber length degradation as a function of residence time. Hence, the overall kinetic can be observed and general conclusions can be drawn.

Table II. Experimental plan1: Impact of residence time and shear rate on length decay

Variable	Levels
Fiber content [%wt]	30
Melt temperature [°C]	250
Rotational speed [rpm]	50, 100
Residence time [s]	20 to 300

2.2.2 Steady state length

The second set of experiments aimed to study the different impact variables have on the residual fiber length, that is, the length at which no additional amount of shearing time will cause additional fiber breakage; or as described by Shon et al., the fiber length at which there is no more buckling. For each

15 July 2024 18:12:51

ACCEPTED MANUSCRIPT
Physics of Fluids
This is the author's peer reviewed, accepted manuscript. However, the online version of record will be different from this version once it has been copyedited and typeset.
PLEASE CITE THIS ARTICLE AS DOI: 10.1063/5.0058693
AIP Publishing
15 July 2024 18:12:51

variant in this study, the residence time and processing speed were selected to ensure L_∞ was reached based on the results of the first experimental plan (300s). This study was designed as a full factorial DOE with three factors and three levels, as shown in Table III. The melt temperature was varied between 220°C and 280°C, representing the limits of the processing temperature range suggested by the material supplier. Hence, the obtained measurements represent the most severe impact that can be expected from this factor.

Table III. Experimental plan 2: Impact of process variables on equilibrium length

Variable	Levels
Fiber content [%wt]	20, 30, 40
Melt temperature [°C]	220, 250, 280
Rotational speed [rpm]	50, 100, 150
Residence time [s]	300

2.2.3 Attrition rate

This third set of experiments aims to identify the influence processing conditions have on the initial breakage rate. Based on the exponential decay kinetics observed in previous studies, the most significant fiber length change occurs early in the shearing cycle. Hence, fiber length measurements at the start of shearing would provide the best insights into the dynamic behavior.

The goal of modeling fiber attrition in this work is aimed for a homogeneous suspension. Consequently, the fact that the fibers and matrix are not mixed in the initial pellet introduces additional variability into the study. To illustrate this fact, Figure 3 shows a sequence of x-ray micro-computed tomography (μCT) images of PPGF40 pellets before shearing and after 5s, 12s, and 20s of shearing. It is evident that perhaps a heterogeneous mixture of fiber bundles and polymer matrix is present before 12s rather than a suspension as observed at 20s.

ACCEPTED MANUSCRIPT
Physics of Fluids
This is the author's peer reviewed, accepted manuscript. However, the online version of record will be different from this version once it has been copyedited and typeset.
PLEASE CITE THIS ARTICLE AS DOI: 10.1063/5.0058693
AIP Publishing

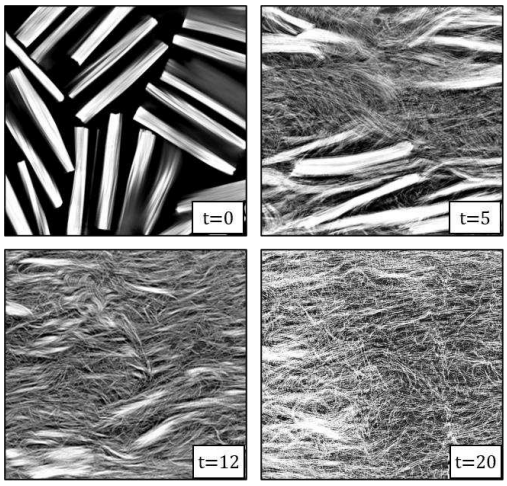

Figure 3. µCT slices of fiber dispersion for PPGF40 exposed to a simple shear flow at $50s^{-1}$ for different residence times.

To address the issue of initial heterogeneity, a pre-dispersion step was introduced to disperse the bundle of fibers without causing excessive damage. This step involved shearing the polymer melt for 2s with a shear rate of $50s^{-1}$. After pre-dispersion, the sample was sheared for 2 additional seconds at higher shear rates as part of the actual experiment. The experiments were performed using a high acceleration rate Couette rheometer at SABIC Technology Center in Geleen, The Netherlands. With this equipment, high deformation rates could be imposed on the polymer melt for short periods. The temperature remained constant, while fiber content and processing speed were varied, as shown in Table IV.

Table IV. Experimental plan 3: Impact of shear rate and fiber concentration on attrition rate.

Variable	Levels
Fiber content [%wt]	20, 30, 40
Melt temperature [°C]	250
Shear rate [s^{-1}]	300, 500, 700
Residence time [s]	2

3 Results

The results are presented in three sections corresponding to the three experimental studies. When evaluating the results, fiber length is presented in terms of the weight-average L_W. The number-average fiber length (L_N) is also needed to reconstruct the FLD; however, as both variables show the same trends with respect to the processing parameters, the results are presented in terms of L_W as it is more representative of the length variable in LFTs.

15 July 2024 18:12:51

ACCEPTED MANUSCRIPT
Physics of Fluids
This is the author's peer reviewed, accepted manuscript. However, the online version of record will be different from this version once it has been copyedited and typeset.
PLEASE CITE THIS ARTICLE AS DOI: 10.1063/5.0058693
AIP Publishing
15 July 2024 18:12:51

3.1 Average length decay over time

Figure 4 shows the fiber length reduction as a function of residence time for PPGF30 with a melt temperature of 250°C at different shearing speeds. For these processing conditions, L_W decreased from 15 mm down to 1.6 mm and 0.75 mm with Couette rotational speeds of 50 rpm and 100 rpm, respectively. Overall, the results confirm the expected exponential decay with a severe length reduction of the fibers occurring within the first 50s of processing. As expected, an increment in processing speed increases the fibers break rate and decreases the residual/equilibrium length [18,26].

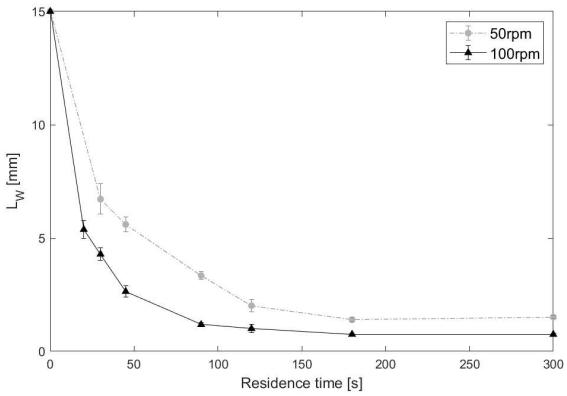

Figure 4. Fiber length reduction over time for PPGF30 at 250°C

3.2 Steady-state length

The investigation of the processing conditions and fiber concentration on the unbreakable fiber length, L_∞, allows direct analysis of the mechanisms that drive fiber damage because it excludes the transient attrition at lower residence times. Figure 5 presents the results of the DOE showing the unbreakable length as the weight-average fiber length.

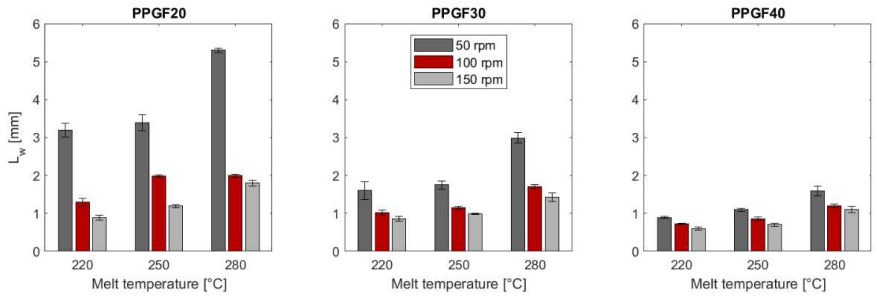

Figure 5. Outcome of the DOE for the steady state length showing the obtained weight-average fiber length $\boldsymbol{L_{W\infty}}$

ACCEPTED MANUSCRIPT
Physics of Fluids
This is the author's peer reviewed, accepted manuscript. However, the online version of record will be different from this version once it has been copyedited and typeset.
PLEASE CITE THIS ARTICLE AS DOI: 10.1063/5.0058693
AIP Publishing
15 July 2024 18:12:51

An analysis of variance was applied to the measurements to determine differences in means between the factors and the level of the DOE factors. Figure 6 shows the main effect plots with respect to $L_{W\infty}$. All three factors influence $L_{W\infty}$ and have a statistically significant impact on the process-induced fiber breakage.

The melt temperature affects the suspension viscosity and, consequently, the stresses that the fibers are exposed to during processing. This dependency is evident in the obtained results, as the increase in temperature results in longer equilibrium length across all other factors. Additionally, processing speed also had the expected effect on the equilibrium length as the rate of deformation increases the hydrodynamic stress experienced by the fibers, forcing the equilibrium length to go down. In all trials, an increased fiber concentration resulted in reduced $L_{W\infty}$. An increment in fiber content implies an increase in one of the breakage mechanisms, namely, fiber-fiber interactions. This result is essential since it indicates that fiber concentration is an essential variable in the kinetics of fiber attrition and the controlled conditions of the experimental setup allow for a clean incorporation into the modeling.

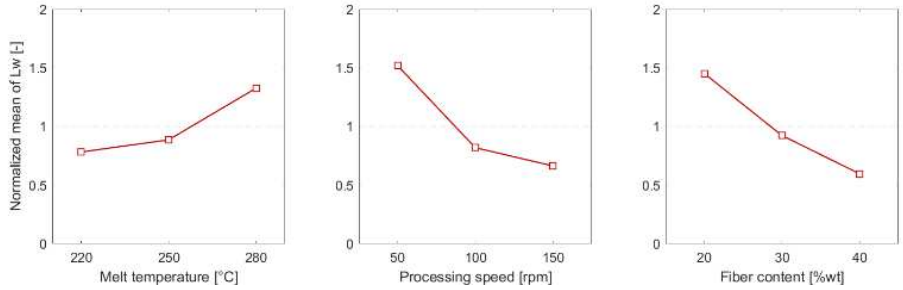

Figure 6. Result of the statistical analysis showing main effect plots on $\boldsymbol{L_{W\infty}}$

3.3 Attrition rate

Figure 7 shows the decrease in length for a short period for PPGF20, PPGF30, and PPGF40. Here, the pre-dispersion step's impact is evident; the length was reduced from its initial value of 15 mm to 7 mm approximately. However, it is still constant for each fiber concentration which is necessary for the subsequent analysis.

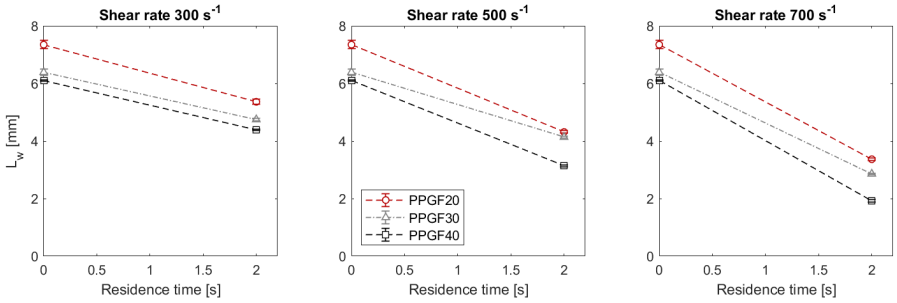

Figure 7. Outcome of experimental plan 3 showing the effect of shear rate on fiber attrition rate.

ACCEPTED MANUSCRIPT
Physics of Fluids
This is the author's peer reviewed, accepted manuscript. However, the online version of record will be different from this version once it has been copyedited and typeset.
PLEASE CITE THIS ARTICLE AS DOI: 10.1063/5.0058693
AIP Publishing

As observed in the first study, the attrition rate increases with the rate of deformation, and the fiber length after shearing the sample at 700 s^{-1} is nearly half of the length after shearing at 300 s^{-1}. Although the slope depends on the initial length and the initial length changes between fiber concentrations, it can be observed that the lines are nearly parallel, which suggests that the fiber content might not have a strong impact on the fibers' initial break rate.

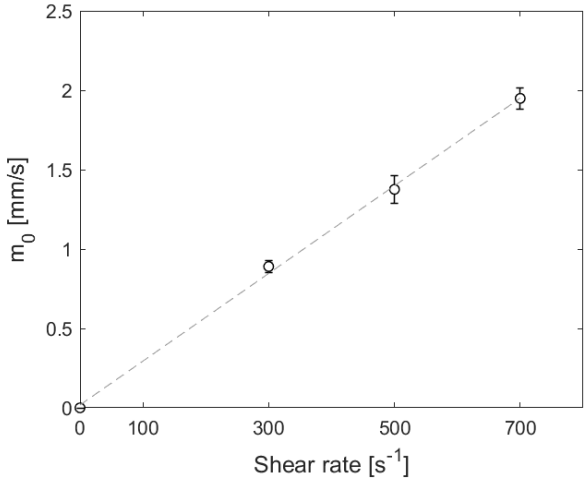

Figure 8. Average initial slope as a function of shear rate. Dashed line shows linear fit with R^2=0.998

Plotting the absolute value of the average initial slope as a function of the shear rate shows a linear proportionality between the variables, especially when including the data point at the origin; since if the fibers are subjected to no shear, there will be no damage, and the slope will be zero (Figure 8).

4 Model development

Based on the analysis of the experimental results and reviewed previews work, the main arguments for the development of a new modeling approach for stress-induced fiber damage are presented.

I. Von Turkovich et al. conducted studies on the compounding of SFTs employing a single screw extruder [13]. One main conclusion was that fiber content does not have a significant effect on fiber attrition. Partly based on their conclusion, Phelps et al. neglected fiber interactions as a source of damage and defined buckling as the sole mechanism for triggering failure [20,35]. However, high stresses and complex flow conditions present during the extrusion process make it hard to establish direct correlations between fiber length and individual factors confidently.

II. While the hydrodynamic stresses will cause buckling, which might lead to failure in short fibers; on average, much larger deformations are needed to cause breakage of the E-glass fibers commonly used in LFTs (D≈20μm). Salinas and Pittman show that fibers can reach large deformations, far past the point of buckling before finally breaking [17]. Additionally, critical radii measurements via loop test for E-glass fibers showed that very small curvatures could be reached before a fracture occurs [28].

15 July 2024 18:12:51

ACCEPTED MANUSCRIPT
Physics of Fluids
This is the author's peer reviewed, accepted manuscript. However, the online version of record will be different from this version once it has been copyedited and typeset.
PLEASE CITE THIS ARTICLE AS DOI: 10.1063/5.0058693
AIP Publishing
15 July 2024 18:12:51

III. The experiments under controlled processing conditions employing the Couette rheometer showed a significant correlation between fiber volume fraction and the steady-state length [26]. While Moritzer concluded that fiber content impacts both the attrition rate and the steady-state length, the experimental result of this work suggests the fiber volume fraction has a weak impact on the attrition rate.

We postulate the average fiber length reduction over time follows an exponential decay towards an equilibrium value as suggested by Shon et al. [18]. A state equation can then be written for each length average L_N and L_W. This will allow for the reconstruction of the fiber length distribution at any point in time.

$$\frac{dL_N}{dt} = -k_{N,f}(L_N - L_{N\infty}) \quad (3)$$

$$\frac{dL_W}{dt} = -k_{W,f}(L_W - L_{W\infty}) \quad (4)$$

We now move on to deriving expressions for both parameters of the state equation L_∞ and k_f.

4.1 Equilibrium length

Describing the fundamental attrition mechanism as a single fiber undergoes bending deformation caused by the hydrodynamic drag of the moving melt, the fiber could be assumed as a cantilever beam under a distributed load. This fiber held by perhaps a group of neighboring fibers or the walls of the barrel or screw can be at the brink of rupture at the length, L_∞, due to the distributed load, as depicted in Figure 9.

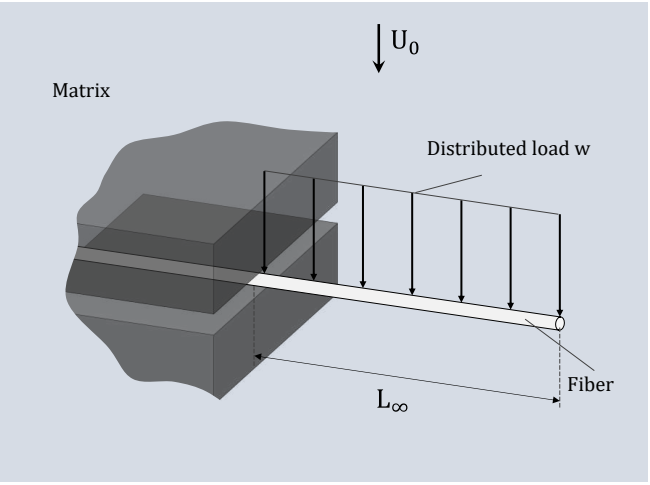

Figure 9. Illustration of a fiber experiencing distributed load due to drag force

ACCEPTED MANUSCRIPT
Physics of Fluids
This is the author's peer reviewed, accepted manuscript. However, the online version of record will be different from this version once it has been copyedited and typeset.
PLEASE CITE THIS ARTICLE AS DOI: 10.1063/5.0058693
AIP Publishing
15 July 2024 18:12:51

The hydrodynamic load exerted by the melt flow on the cylindrical body is based on Stokes law by approximating the cantilever length as a chain of spheres with equal diameter [36]. The load w per unit length is calculated as:

$$w = 3\pi\eta_m U_o \tag{5}$$

where η_m is the matrix viscosity and U_o is the uniform speed of the melt. Which leads to maximum hydrodynamic stress at the base of:

$$\sigma_{max} = \frac{48\eta_m U_o L^2}{d_f^3} \tag{6}$$

with L and d_f as the cantilever length and fiber diameter, respectively. When the stress reaches the fiber's ultimate strength, failure occurs. This leads to the following expression for the critical, or unbreakable length L_∞:

$$L_\infty = \left(\frac{\sigma_{ut} d_f^3}{48\eta_m U_o}\right)^{1/2} \tag{7}$$

The characteristic shear rate can be defined as $\dot{\gamma} = U_0/h$, where h is introduced to describe a characteristic distance, such as channel depth, runner size, or cavity thickness.

$$L_\infty = \left(\frac{\sigma_{ut} d_f^3}{48\eta_m \dot{\gamma} h}\right)^{1/2} \tag{8}$$

Assuming that h is proportional to d_f, $h \propto d_f$, so that:

$$L_\infty \propto \left(\frac{\sigma_{ut} d_f^2}{48\eta_m \dot{\gamma}}\right)^{1/2} \tag{9}$$

The proportionality can be resolved by introducing a dimensionless constant, λ, which gives:

$$L_\infty = \lambda\left(\frac{\sigma_u\, d_f^2}{\eta_m \dot{\gamma}}\right)^{1/2} \tag{10}$$

ACCEPTED MANUSCRIPT
Physics of Fluids
This is the author's peer reviewed, accepted manuscript. However, the online version of record will be different from this version once it has been copyedited and typeset.
PLEASE CITE THIS ARTICLE AS DOI: 10.1063/5.0058693
AIP Publishing
15 July 2024 18:12:51

The coefficient λ is a material-dependent property and a measure of fiber interactions that cause fiber attrition during processing. The parameter is assumed to capture the effects of fiber concentration (fiber-fiber interactions) and fiber-wall interactions. Figure 10 shows the interaction coefficient λ as a function of fiber content as obtained from the measured $L_{W\infty}$ values of the Couette rheometer experiments.

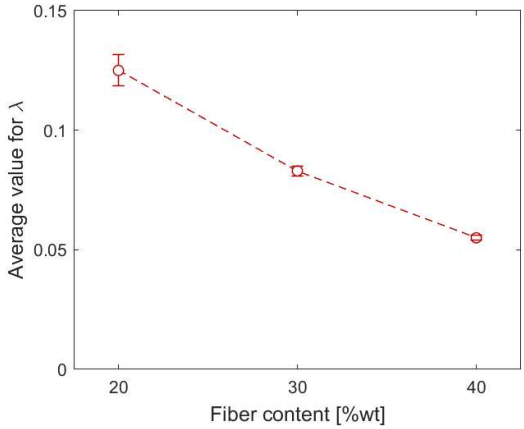

Figure 10. Average interaction coefficient λ as function of fiber concentration

4.2 Breakage rate

The parameter k_f can also be calculated from the Couette rheometer experiments. As seen in Figure 11, an analysis of variance was applied to k_f to determine its variation with respect to fiber concentration and shear rate. While the fiber concentration does not have a statistically significant impact on the breakage rate coefficient, the shear rate does.

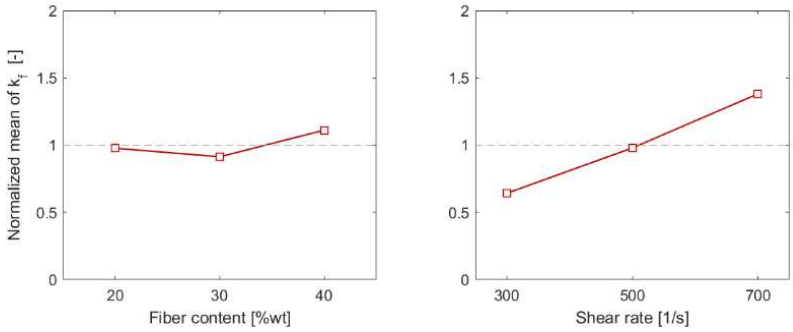

Figure 11. Result of the statistical analysis showing main effect plots on $\boldsymbol{k_f}$

ACCEPTED MANUSCRIPT
Physics of Fluids
This is the author's peer reviewed, accepted manuscript. However, the online version of record will be different from this version once it has been copyedited and typeset.
PLEASE CITE THIS ARTICLE AS DOI: 10.1063/5.0058693
AIP Publishing
15 July 2024 18:12:51

In the current modeling approach k_f represents how often fibers will reach the critical conditions described in the formulation of L_∞. Similar to the fiber-fiber interaction in the Folgar-Tucker model [37], it can be argued that this frequency is proportional to the amount of fiber motion, $k_f \propto \dot{\gamma}$, caused by the flow as described by Forgacs and Salinas [17]. The linear correlation between $\dot{\gamma}$ and k_f shown in Figure 11, leads to a straightforward expression for the breakage rate coefficient:

$$k_f = \xi \dot{\gamma} \quad (11)$$

where ξ is a scale factor for the rate of deformation.

In work by Wolf and Gupta et al., fiber length was measured along the melting zone of a single screw extruder [38,39]. Both researchers observed that a large population of very short fibers originated from the damage occurring at the interface between the bed of solids and the melt pool. In contrast, moderate fiber damage was observed inside the melt pool where fibers were already dispersed and fully surrounded by the matrix. This points to the presence of different damage mechanisms during plastication. When full bundles are present, fiber damage happens mainly at the ends of these bundles, when the drag flow shears off the tips of the fibers (Figure 12,a); but when fibers are fully surrounded by matrix, drag forces cause deformation which leads to damage (Figure 12,b).

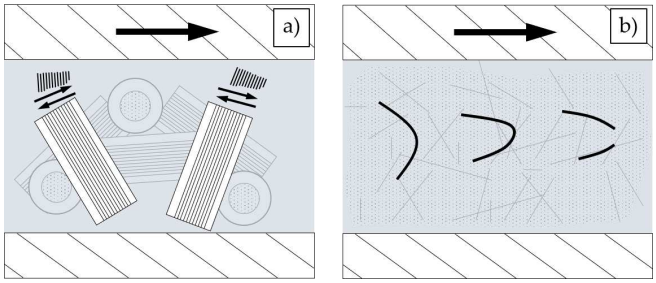

Figure 12 Illustration of fiber breakage mechanisms under different dispersion stages a) undispersed fiber bundles, b) fully dispersed fibers

The attrition rate coefficient k_f, is a measurement of how regularly breakage occurs. Therefore, in the presence of two different damage mechanisms, the attrition rate coefficient k_f will undergo a transition as the flow condition evolves from a heterogenous mix of bundles and matrix, to a fully dispersed suspension. To evaluate the effect fiber dispersion can have on the breakage rate , the results obtained from the Couette experiments are used. First, the value for ξ_W can be recovered from the attrition rate experiment, where the pre-dispersion step ensures damage occurred predominantly due to fiber motion and deformation as illustrated in Figure 12,b. this results in a value of $\xi_W = 4.66\times10^{-4}$. Similarly, by fitting equation 1 to the experimental data presented in Figure 4, the value for $k_{f,W}$ and ξ_W can be calculated. In this case, the shearing process started when the fiber bundles were undispersed, mainly leading to the type of damage illustrated in Figure 12,a. This results in a value of $\xi_W = 1.21\times10^{-3}$. This simple comparison suggests that fiber breakage occurs much more often when the fibers are not well dispersed.

ACCEPTED MANUSCRIPT
Physics of Fluids
This is the author's peer reviewed, accepted manuscript. However, the online version of record will be different from this version once it has been copyedited and typeset.
PLEASE CITE THIS ARTICLE AS DOI: 10.1063/5.0058693
AIP Publishing

4.3 Constitutive model

The proposed model uses two fitting parameters: ξ, which scales $\dot{\gamma}$ in the breakage rate formulation and the interaction coefficient λ, which encapsulates the effects of fiber interactions and is a function of the fiber concentration. An independent set of fitting parameters must be used for the constitutive equations in terms of L_N and L_W. The definition of both parameters in terms of processing conditions and material properties allows for the constitutive equations to be written in terms of the total derivative and implemented in a cavity filling simulation where the flow field information is used to calculate the model constants to predict the fiber length.

$$\frac{dL_N}{dt} + (u \cdot \nabla)L_N = -k_{f,N}(L_N - L_{N,\infty}) \quad (12)$$

$$\frac{dL_W}{dt} + (u \cdot \nabla)L_W = -k_{f,W}(L_W - L_{W,\infty}) \quad (13)$$

To test the performance of the proposed model, its prediction can be compared to fiber length measurements from the Couette studies. Since the fiber length measurements from various Couette studies were used to find the fitting parameters $\lambda(\phi)$ and ξ, an independent set Couette experiments, similar to those presented in Figure 4 will be used as reference for comparison. However, since the initial sample is composed of undispersed bundles, the parameters ξ_N and ξ_W used in this validation correspond to the values determined from the experiments where the fibers were initially undispersed at the start of the shearing cycle. The processing conditions for the reference Couette experiments are listed in Table V.

Table V. Process conditions of Couette experiment for model validation

Parameter	Value
Melt Temperature [°C]	222
Residence time [s]	30-300
Fiber concentration [%wt]	30
Speed [rpm]	160

These processing conditions are rather extreme since the temperature is near the lowest value recommended by the material supplier and the rotational speed was set to the higher limit of the Brabender Plasti Corder™ torque rheometer. This places the processing conditions right at the bound of the design space from the fiber breakage DOE. When modeling the flow in the Couette rheometer, the velocity profile is constant and there are no changes in the z and θ directions, therefore, the convective terms in equations (12) and (13) are not included and the length decay follows equations (3) and (4).

15 July 2024 18:12:51

ACCEPTED MANUSCRIPT
Physics of Fluids
This is the author's peer reviewed, accepted manuscript. However, the online version of record will be different from this version once it has been copyedited and typeset.
PLEASE CITE THIS ARTICLE AS DOI: 10.1063/5.0058693
AIP Publishing

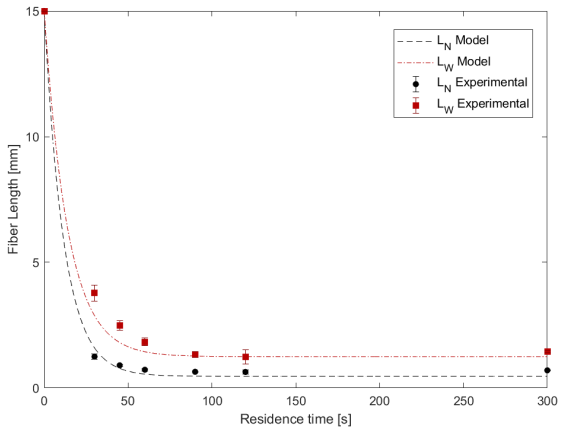

Figure 13 Comparison between fiber length decay obtained with the Couette rheometer and fiber predicted with the proposed model

The comparison between experimental and predicted fiber length is presented in Figure 13. As expected, the equilibrium length is well captured by the model for both length averages L_N and L_W. It is difficult to establish comparisons in the dynamic portion of the length decay since there are few experimental points. However, it can be observed the rate of attrition shows a good agreement for L_N, but it seems to be overpredicted for L_W. Normally, L_N measurements have lower standard deviation than L_W, and this is reflected in the estimation of the fitting parameter ξ_W. Nevertheless, the model captures the overall behavior well.

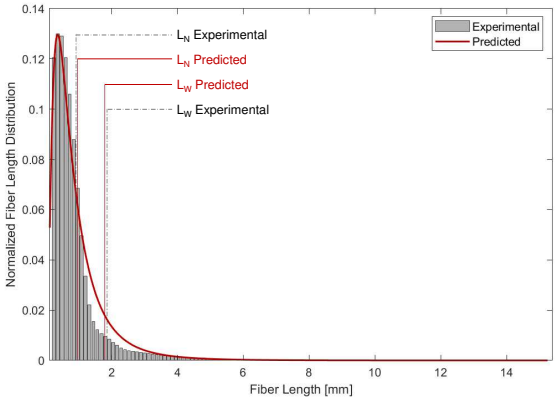

Figure 14 Recovered fiber length distribution employing Log-normal PDF versus experimental fiber length distribution

15 July 2024 18:12:51

ACCEPTED MANUSCRIPT
Physics of Fluids
This is the author's peer reviewed, accepted manuscript. However, the online version of record will be different from this version once it has been copyedited and typeset.
PLEASE CITE THIS ARTICLE AS DOI: 10.1063/5.0058693
AIP Publishing
15 July 2024 18:12:51

Using L_N and L_W as two moments of the fiber length distributioin function, a predicted fiber length distribution is computed using a Log-normal probability density function (PDF) given by

$$f(x) = \frac{1}{x\sigma\sqrt{2\pi}} \exp\left(\frac{(\ln x - \mu)^2}{2\sigma^2}\right) \quad (14)$$

The resulting PDF is presented in Figure 14. Work by Nguyen et al. shows that this PDF can closely reproduce the FLD and yield elastic constants very close to those obtained from experimental measurements [40]. However, the authors noted that when using this probability distribution, the quantity of mid-range fiber lengths is often overpredicted. This can also be observed in our results, as the continuous distribution diverts form the experimental data near the 2 mm mark. This discrepancy has little to no effect in the predicted elastic constants, however in can have more impact in the prediction of the ultimate strength and impact strength.

5 Conclusions

Fiber breakage under simple shear experiments was conducted by employing a Couette rheometer and investigating the influence of fiber concentration, rate of deformation, and viscosity in breakage kinetics. Based on the experimental observations, a continuum approach is developed to predict the fiber length averages L_N and L_W. A model for the equilibrium length (L_∞) is deduced, using the concept that fibers break by bending under hydrodynamically-induced forces and fiber-fiber interactions. The breakage rate coefficient (k_f) is associated with fiber motion and therefore modeled proportionally to the rate of deformation. Finally, both length averages are used to recover the fiber length distribution employing a Weibull or log-normal PDF.

Some of the obtained experimental results contradict previous assertions on fiber-fiber interactions' role in fiber breakage phenomena. Bailey and kraft observed an increase in fiber length with a 20%wt increment in fiber concentration in moldings with PA66 and PP, while von Turkovich et al. concluded fiber concentration had no impact on fiber damage. Using a Couette device to impose simple shear on the suspension, this work looks to remove the complexities present during molding and extrusion processes, allowing us to isolate individual factors' role on fiber breakage. However, it is important to identify the different breakage mechanisms present as the fibers disperse into a homogeneous suspension.

There are similarities between the model presented in this work and the model by Phelps et al. In their work, they derive an unbreakable length, L_∞ (or L_{ub}):

$$L_\infty = \left[\frac{\pi^3 E_f d_f^4}{4\,\zeta \eta_m \dot{\gamma}}\right]^{1/4} \quad (15)$$

This expression represents an equilibrium between internal resistance of the fiber ($E_f d_f$) and external stresses ($\eta_m \dot{\gamma}$), as does the expression of (Eq. (10). However, the model presented in this work assigns more weight to the product $\eta_m \dot{\gamma}$ on account of the exponent ½ versus ¼ in their model. In their model,

ACCEPTED MANUSCRIPT
Physics of Fluids
This is the author's peer reviewed, accepted manuscript. However, the online version of record will be different from this version once it has been copyedited and typeset.
PLEASE CITE THIS ARTICLE AS DOI: 10.1063/5.0058693
AIP Publishing

the overall rate of reduction of fiber length scales with $C_B\dot{\gamma}$, which is equivalent to the expression $k_f = \xi\dot{\gamma}$ used in the model presented in this work. Furthermore, the values obtained for ξ after fitting k_f to the Couette results (1×10^{-3} - 4×10^{-4}) fall within the range suggested for C_B in previous work (2×10^{-2} - 2×10^{-4}) [20,35].

Reducing the number of fitting parameters introduced when developing a model is beneficial since this makes the approach more robust and potentially reduces the number of experiments needed to determine such parameters [41]. Modeling L_N and L_W independently for this case, each constitutive equation has its set of two fitting parameters that are determined from the experimental data. Additionally, a single length measurement provides data for both sets of model parameters.

The proposed model in this work can be implemented into a flow solver for either injection molding or extrusion compounding. Implementation in a mold filling simulation using COMSOL Multiphysics, experimental validation and comparison with other modeling approaches will be the subject of a following publication.

Acknowledgments
The authors wish to thank the National Science Foundation for financially supporting this work (Award #1633967). The authors also thank SABIC Global Technologies B.V. for their financial support, technical input and for providing the material used in this work.

Data Availability
The data that support the findings of this study are available on request from the corresponding author. The data are not publicly available due to company restrictions.

References

[1] H. Ning, N. Lu, A.A. Hassen, K. Chawla, M. Selim, S. Pillay, A review of Long fibre thermoplastic (LFT) composites, Int. Mater. Rev. 65 (2020) 164–188. https://doi.org/10.1080/09506608.2019.1585004.

[2] J. Markarian, Long fibre reinforced thermoplastics continue growth in automotive, Plast. Addit. Compd. 9 (2007) 20–24. https://doi.org/10.1016/S1464-391X(07)70025-9.

[3] U. Gandhi, S. Goris, T.A. Osswald, Y. Song, Understanding Discontinuous Fiber Reinforced Composites - Automotive Applications, Hanser, 2020.

[4] R. Bailey, H. Kraft, A Study of Fibre Attrition in the Processing of Long Fibre Reinforced Thermoplastics, Int. Polym. Process. 2 (1987) 94–101. https://doi.org/10.3139/217.870094.

[5] D. O'Regan, M. Akay, The distribution of fibre lengths in injection moulded polyamide composite components, J. Mater. Process. Technol. 56 (1996) 282–291. https://doi.org/10.1016/0924-0136(95)01842-5.

[6] E. Lafranche, P. Krawczak, J.-P. Ciolczyk, J. Maugey, Injection moulding of long glass fiber reinforced polyamide 66: Processing conditions/microstructure/flexural properties relationship, Adv. Polym. Technol. 24 (2005) 114–131. https://doi.org/10.1002/adv.20035.

[7] M. Rohde, A. Ebel, F. Wolff-Fabris, V. Altstädt, Influence of processing parameters on the fiber

15 July 2024 18:12:51

ACCEPTED MANUSCRIPT
Physics of Fluids
This is the author's peer reviewed, accepted manuscript. However, the online version of record will be different from this version once it has been copyedited and typeset.
PLEASE CITE THIS ARTICLE AS DOI: 10.1063/5.0058693
AIP Publishing

length and impact properties of injection molded long glass fiber reinforced polypropylene, Int. Polym. Process. 26 (2011) 292–303. https://doi.org/10.3139/217.2442.

[8] C. Hopmann, M. Weber, J. Van Haag, M. Schöngart, A validation of the fibre orientation and fibre length attrition prediction for long fibre-reinforced thermoplastics, AIP Conf. Proc. 1664 (2015). https://doi.org/10.1063/1.4918412.

[9] A.B. Senior, T. Osswald, Measuring Fiber Length in the Core and Shell Regions of Injection Molded Long Fiber-Reinforced Thermoplastic Plaques, J. Compos. Sci. 4 (2020) 104. https://doi.org/10.3390/jcs4030104.

[10] S. Goris, T.A. Osswald, Process-induced fiber matrix separation in long fiber-reinforced thermoplastics, Compos. Part A Appl. Sci. Manuf. 105 (2018) 321–333. https://doi.org/10.1016/j.compositesa.2017.11.024.

[11] A. Inoue, K. Morita, T. Tanaka, Y. Arao, Y. Sawada, Effect of screw design on fiber breakage and dispersion in injection-molded long glass-fiber-reinforced polypropylene, J. Compos. Mater. 49 (2015) 75–84. https://doi.org/10.1177/0021998313514872.

[12] K. Kimura, Y. Itamochi, H. Tomiyama, The Evaluation of Mixing Characteristics of Dulmage Screw, Adv. Mater. Res. 747 (2013) 769–772. https://doi.org/10.4028/www.scientific.net/AMR.747.769.

[13] R. von Turkovich, L. Erwin, Fiber fracture in reinforced thermoplastic processing, Polym. Eng. Sci. 23 (1983) 743–749. https://doi.org/10.1002/pen.760231309.

[14] O.L. Forgacs, S.G. Mason, Particle motions in sheared suspensions. IX. Spin and deformation of threadlike particles, J. Colloid Sci. 14 (1959) 457–472. https://doi.org/10.1016/0095-8522(59)90012-1.

[15] O.L. Forgacs, S.G. Mason, Particle motions in sheared suspensions. X. Orbits of flexible threadlike particles, J. Colloid Sci. 14 (1959) 473–491. https://doi.org/10.1016/0095-8522(59)90013-3.

[16] J.M. Burgers, On the motion of small particles of elongated form supended in a viscous fluid, Delft, 1938.

[17] A. Salinas, J.F.T. Pittman, Bending and Breaking Fibers in Sheared Suspensions, Polym. Eng. Sci. 21 (1981) 23–31.

[18] K. Shon, D. Liu, J.L. White, Experimental Studies and Modeling of Development of Dispersion and Fiber Damage in Continuous Compounding, Int. Polym. Process. 20 (2005) 322–331. https://doi.org/10.3139/217.1894.

[19] S.H. Bumm, J.L. White, A.I. Isayev, Glass fiber breakup in corotating twin screw extruder: Simulation and experiment, Polym. Compos. 33 (2012) 2147–2158. https://doi.org/10.1002/pc.22356.

[20] J.H. Phelps, A.I. Abd El-Rahman, V. Kunc, C.L. Tucker, A model for fiber length attrition in injection-molded long-fiber composites, Compos. Part A Appl. Sci. Manuf. 51 (2013) 11–21. https://doi.org/10.1016/j.compositesa.2013.04.002.

[21] A. Durin, P. De Micheli, J. Ville, F. Inceoglu, R. Valette, B. Vergnes, A matricial approach of fibre breakage in twin-screw extrusion of glass fibres reinforced thermoplastics, Compos. Part A Appl. Sci. Manuf. 48 (2013) 47–56. https://doi.org/10.1016/j.compositesa.2012.12.011.

15 July 2024 18:12:51

ACCEPTED MANUSCRIPT
Physics of Fluids
This is the author's peer reviewed, accepted manuscript. However, the online version of record will be different from this version once it has been copyedited and typeset.
PLEASE CITE THIS ARTICLE AS DOI: 10.1063/5.0058693
AIP Publishing

[22] J. Kang, M. Huang, M. Zhang, N. Zhang, G. Song, Y. Liu, X. Shi, C. Liu, An effective model for fiber breakage prediction of injection-molded long fiber reinforced thermoplastics, J. Reinf. Plast. Compos. 39 (2020) 473–484. https://doi.org/10.1177/0731684420915643.

[23] H. Malatyali, V. Schöppner, N. Rabeneck, F. Hanselle, L. Austermeier, D. Karch, A model for the carbon fiber breakage along the twin-screw extruder, SPE Polym. 2 (2021) 145–152. https://doi.org/10.1002/pls2.10040.

[24] H. Chen, M. Cieslinski, P. Wapperom, D.G. Baird, Long fiber (glass) breakage in capillary and contraction flow, Annu. Tech. Conf. - ANTEC, Conf. Proc. (2015) 546–550.

[25] J.H. Phelps, C.L. Tucker, An anisotropic rotary diffusion model for fiber orientation in short- and long-fiber thermoplastics, J. Nonnewton. Fluid Mech. 156 (2009) 165–176. https://doi.org/10.1016/j.jnnfm.2008.08.002.

[26] E. Moritzer, H. Gilmar, Fiber Length Degradation of Glass Fiber Reinforced Polypropylene During Shearing, in: SPE ANTEC, 2016: pp. 647–651.

[27] T. Sasayama, M. Inagaki, N. Sato, Direct simulation of glass fiber breakage in simple shear flow considering fiber-fiber interaction, Compos. Part A Appl. Sci. Manuf. 124 (2019) 105514. https://doi.org/10.1016/j.compositesa.2019.105514.

[28] T.-C. Chang, A. Bechara Senior, H. Celik, D. Brands, A. Yanev, T. Osswald, Validation of Fiber Breakage in Simple Shear Flow with Direct Fiber Simulation, J. Compos. Sci. 4 (2020) 134. https://doi.org/10.3390/jcs4030134.

[29] L. Nippon Electric Glass Co., E Glass Fiber – Direct Roving Product List, (2021). https://www.neg.co.jp/en/product/e-roving_list/ (accessed May 6, 2021).

[30] NetComposites, Volume-Weight Fraction Calculator, (2019). https://netcomposites.com/calculator/volume-weight-fraction-calculator/ (accessed May 6, 2021).

[31] 3B - the fibreglass company, TYPICAL 3B E-CR GLASS PROPERTIES, (n.d.). https://www.3b-fibreglass.com/3b-e-glass (accessed May 6, 2021).

[32] S. Goris, S. Simon, C. Montoya, A. Bechara, M.V. Candal, D. Brands, A. Yanev, T.A. Osswald, Experimental study on fiber attrition of long glass fiber-reinforced thermoplastics under controlled conditions in a couette flow, in: Annu. Tech. Conf. - ANTEC, Conf. Proc., 2017.

[33] S. Goris, T. Back, A. Yanev, D. Brands, D. Drummer, T.A. Osswald, A novel fiber length measurement technique for discontinuous fiber-reinforced composites: A comparative study with existing methods, Polym. Compos. 39 (2018) 4058–4070. https://doi.org/10.1002/pc.24466.

[34] V. Kunc, B. Frame, B.N. Nguyen, C.L. Tucker, G. Velez-Garcia, Fiber length distribution measurement for long glass and carbon fiber reinforced injection molded thermoplastics, SPE Automot. Compos. Div. - 7th Annu. Automot. Compos. Conf. Exhib. ACCE 2007 - Driv. Perform. Product. 2 (2007) 866–876.

[35] J.H. Phelps, Processing-Microstructure Models for Short- and Long-Fiber Thermoplastic Composites, University of Illinois at Urbana-Champaign, 2009.

[36] D. Ramirez, Study of Fiber Motion in Molding Processes by Means of a Mechanitic Model,

15 July 2024 18:12:51

ACCEPTED MANUSCRIPT
Physics of Fluids
AIP Publishing
This is the author's peer reviewed, accepted manuscript. However, the online version of record will be different from this version once it has been copyedited and typeset.
PLEASE CITE THIS ARTICLE AS DOI: 10.1063/5.0058693

University of Wisconsin-Madison, 2014.

[37] F. Folgar, C.L. Tucker, Orientation Behavior of Fibers in Concentrated Suspensions., J. Reinf. Plast. Compos. 3 (1984) 98–119. https://doi.org/10.1177/073168448400300201.

[38] H.J. Wolf, Screw plasticating of discontinuous fiber filled thermoplastic: Mechanisms and prevention of fiber attrition, Polym. Compos. 15 (1994) 375–383. https://doi.org/10.1002/pc.750150508.

[39] V.B. Gupta, R.K. Mittal, P.K. Sharma, G. Mennig, J. Wolters, Part I : Reduction in Fiber Length During Processing, Polym. Compos. (1989) 8–15. https://doi.org/10.1007/s10040-016-1436-5.

[40] B. Nghiep Nguyen, S.K. Bapanapalli, V. Kunc, J.H. Phelps, C.L. Tucker, Prediction of the Elastic—Plastic Stress/Strain Response for Injection-Molded Long-Fiber Thermoplastics, J. Compos. Mater. 43 (2009) 217–246. https://doi.org/10.1177/0021998308099219.

[41] F. Dyson, A meeting with Enrico Fermi., Nature. 427 (2004) 297. https://doi.org/10.1038/427297a.

15 July 2024 18:12:51